magnetochemistry

MDPI

Article

Cobalt(II) and Nickel(II) Cubane $\{M_4O_4\}$ Complexes Derived from Di-2-pyridyl Ketone and Benzoate: Syntheses, Structure and Magnetic Properties †

Carolina Pejo [1], Santiago Valiero [1], Carlos Rojas-Dotti [1], Guilherme P. Guedes [2], Joan Cano [3], Miguel A. Novak [4], Raúl Chiozzone [1], Maria G. F. Vaz [2,*] and Ricardo González [1,*]

[1] Facultad de Química, Universidad de la República, General Flores 2124, Montevideo UY-11800, Uruguay; cpejo@fq.edu.uy (C.P.); svaliero@fq.edu.uy (S.V.); carlosrojas@fq.edu.uy (C.R.-D.); rchiozzo@fq.edu.uy (R.C.)
[2] Instituto de Química, Universidade Federal Fluminense, Niterói 24020-150, RJ, Brazil; guilherme_guedes@id.uff.br
[3] Instituto de Ciencia Molecular (ICMol), Universitat de València, 46980 Paterna, València, Spain; joan.cano@uv.es
[4] Instituto de Física, Universidade Federal Fluminense, Niterói 24210-240, RJ, Brazil; miguelnovak@id.uff.br
* Correspondence: mariavaz@id.uff.br (M.G.F.V.); rgonzale@fq.edu.uy (R.G.)
† With this article, we would like to contribute to the well-deserved tribute to the extensive and outstanding academic careers of Paco and Miguel (sadly, Miguel passed away in July 2024), brilliant researchers who made fundamental contributions to coordination chemistry and molecular magnetism. Beyond this we also celebrate them as the extraordinary individuals—extremely generous and always willing to give a helping hand. We are deeply grateful for their friendship, unwavering support, collaboration and the enriching and joyful moments we shared. Thank you Paco and Miguel.

Abstract: Two tetranuclear complexes were obtained by a self-assembly process employing di-2-pyridyl ketone ($(py)_2CO$), benzoate and $M(NO_3)_2$ (M = Co and Ni). The compounds $[M_4\{(py)_2C(OH)O\}_4(O_2CPh)_4]$, where $\{(py)_2C(OH)O\}^-$ is the monoanion of the *gem*-diol form of $(py)_2CO$, were characterized through single-crystal X-ray diffraction and magnetic measurements. Structural analysis revealed that both complexes possess a $[M_4O_4]$ cubane-like core. A two-*J* model and magnetic anisotropy were employed to analyze the magnetic properties of both compounds. These studies indicate the presence of dominant ferromagnetic interactions within both tetranuclear cores. DFT and CASSCF/NEVPT2 calculations were also performed to support the fitting of experimental magnetic data.

Keywords: cobalt; nickel; crystal structures; cubane complexes; magnetic properties; DFT and CASSCF/NEVPT2 calculations

check for updates

Academic Editor: Ming-Liang Tong

Received: 1 March 2025
Revised: 4 April 2025
Accepted: 8 April 2025
Published: 15 April 2025

Citation: Pejo, C.; Valiero, S.; Rojas-Dotti, C.; Guedes, G.P.; Cano, J.; Novak, M.A.; Chiozzone, R.; Vaz, M.G.F.; González, R. Cobalt(II) and Nickel(II) Cubane $\{M_4O_4\}$ Complexes Derived from Di-2-pyridyl Ketone and Benzoate: Syntheses, Structure and Magnetic Properties. *Magnetochemistry* **2025**, *11*, 34. https://doi.org/10.3390/magnetochemistry11040034

1. Introduction

Polynuclear metal complexes have attracted interest in the context of molecular magnetism for more than three decades. Early research primarily focused on the study of magnetic interactions in dinuclear complexes; however, the discovery of slow relaxation of magnetization in Mn_{12} [1] triggered the search for novel coordination clusters with diverse topologies and single-molecule magnet (SMM) behavior [2–4]. Serendipity has played a key role as a synthetic strategy that leads to remarkable structural diversity in magnetic systems. This synthetic approach typically involves the use of flexible polydentate organic ligands capable of coordinating two or more metal ions. These ligands often contain hydroxyl groups that can adopt different coordination modes. Since the primary ligand usually does not saturate the coordination sphere of the metal, the solvent molecules or auxiliary organic or inorganic ligands incorporated during synthesis may also coordinate to the metal. Carboxylates are frequently employed as ancillary ligands owing to their ability to act as both

terminal and bridging, with a variety of ligation modes. This versatility adds additional flexibility to the mixed-ligand systems. Although this flexibility complicates predictions regarding the possible outcomes of synthesis, serendipitous self-assembly has allowed researchers to obtain a vast number of coordination clusters with a large diversity of spin topologies and nuclearities. These clusters range from trinuclear structures to systems comprising over tens of metal ions, involving first-row transition metals and lanthanide elements [5–16]. Among this diverse group of compounds, tetranuclear complexes featuring the M_4O_4 cubane core are one of the most reported structures. All first-row transition metals form this type of isolated cubane complexes, nickel being the most prominent. The CCSD database lists over 270 entries for tetranuclear compounds featuring the Ni_4O_4 core. Cobalt has also enriched the library of oxo cubane complexes, for which around 130 Co_4O_4 compounds can be found in the CCSD database. The observation of SMM behavior in some of these Ni and Co complexes has stimulated the extensive study of magnetic properties in these M_4O_4 families of compounds [17–30]. The accidental orthogonality of magnetic orbitals in M_4O_4 cubes may lead to high-spin ground states, which contribute to a significant barrier to magnetization reversal (U), since the upper limit of U is given by $S^2\,|D|$ and $(S^2 - 1/4)\,|D|$ for integer and half-integer spin, respectively. The molecular spin ground state and the anisotropy of the system are influenced by the nature of the ligand system. Zero-field splitting (zfs) anisotropy associated with the individual M^{II} sites and the exchange coupling between them are affected by changes in the coordination sphere of the M^{II} ions and the M−O−M bond angles. For Ni_4O_4 compounds, a clear correlation between the sign and magnitude of the magnetic exchange constant (J) and the M–O–M bond angle has been established [19,31,32]. On the other hand, although several magnetic studies have been conducted on Co_4O_4 compounds, to the best of our knowledge, magnetostructural correlations have not been reported.

Slight variations in the Ni–O–Ni bond angles can induce significant changes in the magnitude and sign of magnetic interactions, potentially altering the spin ground state. Such changes can occur, for example, through the exchange of coordinated solvent molecules [32] or even by more subtle modifications, such as variations in the peripheral halide atoms of the ligands [33]. Also, changes in coordinated solvent molecules or the substitution of a peripheral H atom with a CH_3 group may switch the SMM behavior in cubane complexes [28,32].

Di-2-pyridyl ketone, $(py)_2CO$, has been proven highly effective in the synthesis of coordination clusters. In the presence of a metal ion, the carbonyl group can undergo addition reactions with different nucleophilic agents such as water or alcohols (ROH), and as a result, the species $(py)_2C(OR)(OH)$ (R = H, alkyl, aryl) are obtained (Scheme 1). Upon the deprotonation of the hydroxyl groups, the resulting dianionic $\{(py)_2C(O)_2\}^{2-}$ or the monoanionic $\{(py)_2C(OR)(O)\}^{-}$ species can function as flexible N, N′, O chelating ligands. This flexibility arises from the ability of the negatively charged oxygen atom to bridge two (μ_2) or three (μ_3) metal ions.

Several polynuclear complexes with nuclearities as high as twenty-six metal centers [34] and diverse topologies have been obtained starting with $(py)_2CO$ [35]. For nickel and cobalt, di-2-pyridyl ketone-based complexes with nuclearities of up to eleven and nine, respectively, have been observed, both with acetate as a coligand [36,37]. Particularly, nine different tetranuclear Ni_4O_4 cubane compounds based on $(py)_2CO$—both neutral and cationic—can be found in the CCSD, with different auxiliary ligands such as hydroxylamine, dicyanamide, nitrate, sulfate, acetate, water and methanol. Magnetic studies have been conducted on five of these complexes, revealing competing ferromagnetic and antiferromagnetic interactions, resulting in $S = 0$ or $S = 2$ spin ground states [38–42]. Regarding di-2-pyridyl ketone-based Co_4O_4 cubane compounds, the CCSD shows seven complexes—both neutral and cationic—

in which acetate/water, chloride, acetate and nitrate act as auxiliary ligands. Magnetic properties have been measured for only four of them. Although no data fitting was performed, competing ferro- and antiferromagnetic interactions can be inferred for the compounds $[Co_4\{(py)_2C(OH)O\}_4(NO_3)_3(H_2O)]NO_3$, $[Co_4\{(py)_2C(OH)O\}_4(O_2CMe)_3(H_2O)](ClO_4)\cdot 1.8H_2O$ and $[Co_4\{(py)_2C(OH)O\}_4(O_2CMe)_4]\cdot H_2O$ [37,39,43]. An intermediate $S = 3$ spin ground state was suggested for the latter, while a second hydrated form, $[Co_4\{(py)_2C(OH)O\}_4(O_2CMe)_4]\cdot 7H_2O$, shows antiferromagnetic interactions leading to a non-magnetic ground state [44].

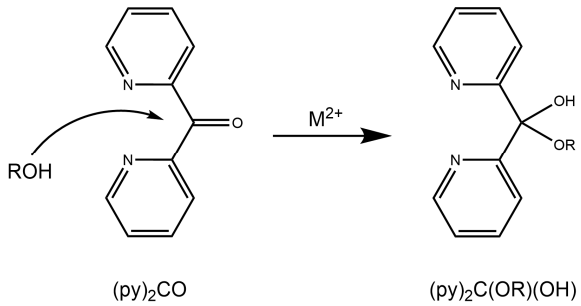

Scheme 1. Di-2-pyridyl ketone $(py)_2CO$ and its neutral *gem*-diol, $(py)_2C(OH)_2$, and hemiketal, $(py)_2C(OR)(OH)$, forms.

Based on the previous discussion about the potential structural diversity and magnetic properties of these systems and taking into account the limited number of studies in which benzoate ($PhCO_2^-$) serves as an auxiliary ligand in $(py)_2CO$-based coordination clusters, we explored the chemistry of $M^{II}/(py)_2CO/PhCO_2^-$ systems, where M = Ni and Co. In this paper, we report the synthesis, crystal structures and both experimental and theoretical studies of magnetic properties of compounds $[M_4\{(py)_2C(OH)O\}_4(O_2CPh)_4]$, where M = Co (**1**) and Ni (**2**). Both compounds present a M_4O_4 cubane core, which exhibits predominant ferromagnetic interactions, leading to high-spin ground states. *Broken-symmetry* DFT and CASSCF/NEVPT2 calculations support these results.

2. Materials and Methods

2.1. Materials and Characterization

All reagents and solvents were purchased from commercial sources and used without further purification. Infrared spectra were recorded with a Shimadzu IR Prestige-21 FTIR spectrometer using KBr pellets from 4000 to 400 cm^{-1}. Elemental analyses of carbon, hydrogen and nitrogen were performed on a Thermo Flash 2000 analyzer.

Magnetic measurements were carried out on polycrystalline samples of **1** and **2** using a Cryogenics SX600 SQUID magnetometer from 2 to 280 K under an applied magnetic field of 1 and 0.1 kOe for **1** and **2**, respectively. The device was calibrated with YFe garnet NIST reference samples. Diamagnetic corrections were estimated from Pascal's constants, and experimental susceptibilities were also corrected for the magnetization of the sample holder.

*2.2. Synthesis of $[Co_4\{(py)_2C(O)(OH)\}_4(O_2CPh)_4]$ (**1**) and $[Ni_4\{(py)_2C(O)(OH)\}_4(O_2CPh)_4]$ (**2**)*

Compound **1** was obtained by adding 73 mg of $Co(NO_3)_2\cdot 6H_2O$ (0.25 mmol) to 10 mL of methanol solution containing NaO_2CPh (0.5 mmol) and 46 mg of $(py)_2CO$ (0.25 mmol). The resulting solution was filtered off and layered with toluene (10 mL). Well-shaped rhombic blue–purple crystals were obtained after 30 days and were filtered off, washed with ethanol and left to dry in air. Yield: 41 mg (34%). *Anal. Calc.* for $[Co_4\{(py)_2C(O)(OH)\}_4(O_2CPh)_4]$ (**2**): C: 56.71; H: 3.69; N: 7.35(%). Found: C: 56.65; H:3.59; N: 7.36 (%). IR (ν/cm^{-1}, KBr): 3494(m), 3416(m), 2800 (m), 1601 (s), 1560 (s), 1387 (s),

1225 (m), 1121 (m), 1071 (m), 1044 (m), 953 (w), 803 (w), 771 (w), 723 (m), 683 (m), 595 (w), 533 (w), 515 (w), 429 (w).

Single crystals of compound **2** were obtained by the same procedure followed for **1** but replacing $Co(NO_3)_2{\cdot}6H_2O$ with $Ni(NO_3)_2{\cdot}6H_2O$. Yield: 50 mg (40%). *Anal. Calc.* for $[Ni_4\{(py)_2C(O)(OH)\}_4(O_2CPh)_4]$ (**1**): C: 56.74; H: 3.69; N: 7.35(%). Found: C: 56.50; H:3.61; N: 7.32 (%). IR (ν/cm^{-1}, KBr): 3500 (m), 3419 (m), 2800 (m), 1601 (s), 1560 (s), 1384 (s), 1223 (m), 1125 (m), 1080 (s), 1045 (m), 1022 (m), 951 (m), 803 (m), 769 (m), 728 (s), 684 (m), 589 (w), 533 (w), 515 (w), 429 (w), 417 (w), 400 (w).

2.3. X-Ray Data Collection and Structure Refinement

Single-crystal X-ray diffraction data were collected on an Xcalibur Atlas Gemini Ultra (**1**) or Bruker KAPPA CCD (**2**) diffractometer using graphite-monochromated Mo Kα radiation (λ = 0.71073 Å) at room temperature. For **1**, CRYSALISPRO software [45] was used to determine the unit cell parameters, the integration of the collected reflections and the absorption correction. The structure solutions and full-matrix least-squares refinements based on F^2 were performed with the SHELXS and SHELXL programs [46]. For **2**, the final unit cell parameters were determined from all reflections obtained with the DIRAX program [47,48], whereas the integration of the collected reflections was performed using the EVALCCD program [49]. Absorption correction using equivalent reflections was performed with the SADABS program [47]. All non-hydrogen atoms were refined anisotropically, while hydrogen atoms were set in calculated positions and refined as riding atoms. Details of the crystal structure, collection and refinement are gathered in Table 1. CCDC numbers 2417037-2417038 contain the supplementary crystallographic data for this article. These data are provided free of charge by the Cambridge Crystallographic Data Centre.

Table 1. Crystal data and structure refinement for compounds **1** and **2**.

Compound	1	2
Empirical formula	$C_{72}H_{56}Co_4N_8O_{16}$	$C_{72}H_{56}N_8Ni_4O_{16}$
Formula weight	1524.97	1524.01
Temperature/K	293(2)	293(2)
Crystal system	Tetragonal	Tetragonal
Space group	I-42d	I-42d
a/Å	14.322(1)	14.172(3)
b/Å	14.322(1)	14.172(3)
c/Å	38.300(1)	37.900(8)
Volume/Å^3	7856.1(11)	7612.1(3)
Z	4	4
ρ_{calc}/g cm^{-3}	1.289	1.330
μ/mm^{-1}	0.895	1.041
F(000)	3120.0	3136.0
Radiation	Mo Kα (λ = 0.71073)	Mo Kα (λ = 0.71073)
2θ range for data collection/°	6.45 to 59.15	10.064 to 50.054
Index ranges	$-18 \leq h \leq 18$ $-19 \leq k \leq 15$ $-51 \leq l \leq 51$	$-16 \leq h \leq 16$ $-16 \leq k \leq 16$ $-42 \leq l \leq 45$
Reflections collected	38328	39546
Independent reflections	5178	3340
R_{int}	0.058	0.081
Data/restraints/parameters	5178/0/215	3340/0/227
Goodness-of-fit on F^2	0.998	1.095
Final R indexes [$I \geq 2\sigma(I)$]	R_1 = 0.0401, wR_2 = 0.1048	R_1 = 0.0437 wR_2 = 0.1215
Final R indexes [all data]	R_1 = 0.0557, wR_2 = 0.1085	R_1 = 0.0530, wR_2 = 0.1290
Largest diff. peak/hole / e Å^{-3}	0.72/−0.32	0.81/−0.34
Flack parameter	−0.011(8)	0.06(4)
CCDC identification	2417038	2417037

2.4. Computational Methodology

All calculations were performed in the ORCA software suite version 5.0.3 [50] using the experimental crystal structure as input. The Def2-tzvp basis set was used for all atoms [51].

Magnetic coupling constants (J) were evaluated by DFT calculations using the Gaussian version of the B3LYP hybrid functional [52,53]. The evaluation of coulomb and exchange two-electron integrals were accelerated using the resolution of identity (RI) and chains of spheres (COSX) [54] approximations with the def2/J auxiliary basis set [55]. A polarizable continuum model (PCM) was introduced in the calculations with parameters corresponding to acetonitrile to reduce the delocalization error typical of DFT methods, mainly in charged systems with close molecular groups and opposite charges [56]. To simplify the calculations, they were carried out on the experimental geometry of M_4, but with the replacement of two paramagnetic M^{II} ions with diamagnetic Zn^{II} ions for each magnetic coupling. According to Ruiz et al. [57–60], magnetic exchange-coupling constants were determined using the *broken-symmetry* approach (BS-DFT). In all cases, a very tight energy convergence threshold was adopted ($\Delta E < 1.0 \times 10^{-9}$ au). Wavefunction stability was verified at each step through ORCA's stability test to ensure convergence to the most stable electronic configuration since the particular local electronic configuration of the Co^{II} ion leads to energetically close excited states [61].

The parameters that determine the axial (D) and rhombic (E) components of the local zero-field splitting (zfs) were estimated from theoretical calculations based on the complete active space self-consistent field method (CASSCF) or through a subsequent second-order N-Electron Valence-State Perturbation Theory (CASSCF/NEVPT2) applied to CASSCF wavefunctions [62–64], which often provides accurate values of the energies of nearby excited states and for the zfs tensor of mononuclear first-row transition metal complexes. For this purpose, MZn3 models were built by replacing three M^{II} ions with diamagnetic Zn^{II} ones. Simple mononuclear models built from the experimental geometries were also studied (see Discussion). For these calculations, J, C and JK auxiliary basis sets were generated automatically [65]. The contributions to zfs of five triplet and ten doublet and ten quartet and twenty doublet excited states for nickel(II) and cobalt(II) models, respectively, generated from an active space with eight (Ni^{II}) or seven (Co^{II}) electrons in five d orbitals, were included through an effective Hamiltonian. The RIJCOSX method was applied by combining the resolution of the identity (RI) and "chain-of-spheres" COSX approximations for the Coulomb and exchange terms [54,66,67].

The magnetic behavior of 1 was analyzed using the XVPMAG package [68], a suite of computational tools designed to efficiently study large and complex systems with varying degrees of precision and methodological approaches. In this study, magnetic susceptibility per tetranuclear M_4 unit (χ_M)-versus-temperature (T) plots were fitted using the Levenberg–Marquardt algorithm [69,70].

For the model incorporating exchange interactions, zero-field splitting (zfs) and the Zeeman effect (Equations (3), (6) and (7), see Section 3.2), the χ_{MT} product was simulated from the energy matrix. The energy matrix built in the basis of Ms functions and of dimensions 256×256 was diagonalized, and the logarithm of the partition function (Z) was computed. Small positive and negative perturbations (ΔH) were applied to derive the second derivative of $\log(Z)$ with respect to H (magnetic field), thus obtaining the magnetic susceptibility. Since measurements were conducted on a solid, unoriented sample, the results were averaged over 30 different orientations. Although fewer than 10 orientations can compromise accuracy, some tests have shown that 30 orientations provide sufficient precision compared to simulations performed using 5×105 randomly generated orientations. Considering the Thomson problem [71,72], care was taken to ensure that the chosen

orientations eliminated any preferential bias by minimizing the electrostatic energy of 30 positive charges positioned on the surface of a sphere.

Additionally, a model incorporating spin-orbit coupling (SOC) for the Co^{II} ion was applied, as described in Equations (2) and (3) (see Section 3.2). This more precise approach involved the diagonalization of a 20,736 × 20,736 energy matrix. While XVPMAG can handle such a large matrix, a simplified theory approach was employed to optimize computational efficiency, which is particularly suitable when the magnetic coupling is not excessively strong. In this method, the SOC effect was resolved using a reduced 12 × 12 energy matrix associating results with local effective spins (S_{eff} = 1/2) and then incorporated into the Hamiltonian governing the magnetic interactions (Equation (3)) for these coupled local effective spins. The most efficient implementation of this approach involved constructing and diagonalizing an energy matrix for each total spin (S_T) using S local basis functions and the irreducible tensor operator (ITO) method [73]. The largest matrix in this process had a dimension of only 3 × 3. Nevertheless, this final diagonalization step could be omitted, as the energy levels of the resulting states for this model are already well established.

The experimental magnetic data for 2 were analyzed using the software package PHI v3.1.6 [74].

3. Results

Compounds **1** and **2** were obtained by reaction of $M(NO_3)_2{\cdot}6H_2O$, $(py)_2CO$ and NaO_2CPh in methanol. This process can be summarized by Equation (1):

$$4M(NO_3)_2{\cdot}6H_2O + 4(py)_2CO + 8NaO_2CPh \rightarrow [M_4\{(py)_2C(OH)O\}_4(O_2CPh)_4] + 8NaNO_3 + 4HO_2CPh + 20H_2O \quad (1)$$

Both complexes contain the monoanionic *gem*-diol form derived from di-2-pyridyl ketone. The formation of this species involves a nucleophilic attack by a water molecule on the carbonyl group of py_2CO (see Scheme 1). Hydration water in metal nitrates and even the moisture in the solvent supply the required amount of water in the reaction mixture for the formation of $(py)_2C(OH)_2$, while the excess of NaO_2Ph facilitates its deprotonation.

The IR spectra of **1** and **2** show medium intense bands in the region of 3500–3400 cm^{-1} that are assigned to the ν(OH) vibration of coordinated $[(py)2C(OH)O]^-$ groups. Other intense bands appear in the region 1600–1380 cm^{-1}, these may be due to contributions from the ν_{as}(C=O) and ν_s(C=O) of $PhCO_2^-$ (1601 cm^{-1} and 1384/1387 cm^{-1}, respectively) and from the stretching vibrations of pyridyl rings (1560 cm^{-1}).

3.1. Structure Description

Compounds **1** and **2** crystallize in the tetragonal I-42d space group and consist of isomorphous systems. Selected bond lengths and angles are listed in Table 2. The asymmetric units are shown in Figure S1 and contain one $\{(py)_2C(OH)O\}^-$ ligand, one benzoate and one M^{2+} cation (M = Co^{2+} (**1**) and Ni^{2+} (**2**)).

The structures consist of neutral tetranuclear $[M_4\{(py)_2C(O)(OH)\}_4(O_2CPh)_4]$ molecules, as can be seen in Figure 1. In both compounds, the metal ions and four oxygen atoms occupy alternated vertices of an S_4 local symmetry $[M_4(\mu_3\text{-}O)_4]$ cubane-like core. Each $\{(py)_2C(OH)O\}^-$ ligand is coordinated to three different metal ions by one oxygen (O1) and two pyridyl nitrogen atoms (N1 and N2). Furthermore, the coordination sphere is filled with one η^1-monodentate benzoate ligand, leading to distorted octahedral geometry around the metal ions. The M–O1 bond lengths are in the range 2.032(2)–2.233(3) Å and 2.005–2.166(4) Å, whereas the M–$O3_{benzoate}$ bond distances are 2.028(3) Å and 2.003(5) Å for **1** and **2**, respectively. As can be seen, the M–O1 lengths are shorter in **2** than in **1**, as expected when comparing nickel(II) and cobalt(II) complexes [75]. These bond lengths fall within the

typical values found for similar compounds featuring the cubane-like motif [21–27]. Moreover, the average M···M distance in the M_4O_4 moiety is shorter for the nickel derivative [3.123(1) Å for **2** vs. 3.2283(8) Å for **1**]. In accordance with the point symmetry exhibited by the M_4O_4 units, the two opposite faces of the cubane that are perpendicular to the S_4 axis are equivalent to each other and distinct from the remaining four side faces. Both sets of faces are characterized by different M···M distances and M−O1−M bond angles. The four side faces show M−O1−M bond angles of 96.17(9)° and 102.61(10)° for **1** and 97.48(16)° and 102.78(17)° for **2**, while bond angles of 97.83(9)° and 95.47(16)° are found for the faces perpendicular to S4 in **1** and **2**, respectively.

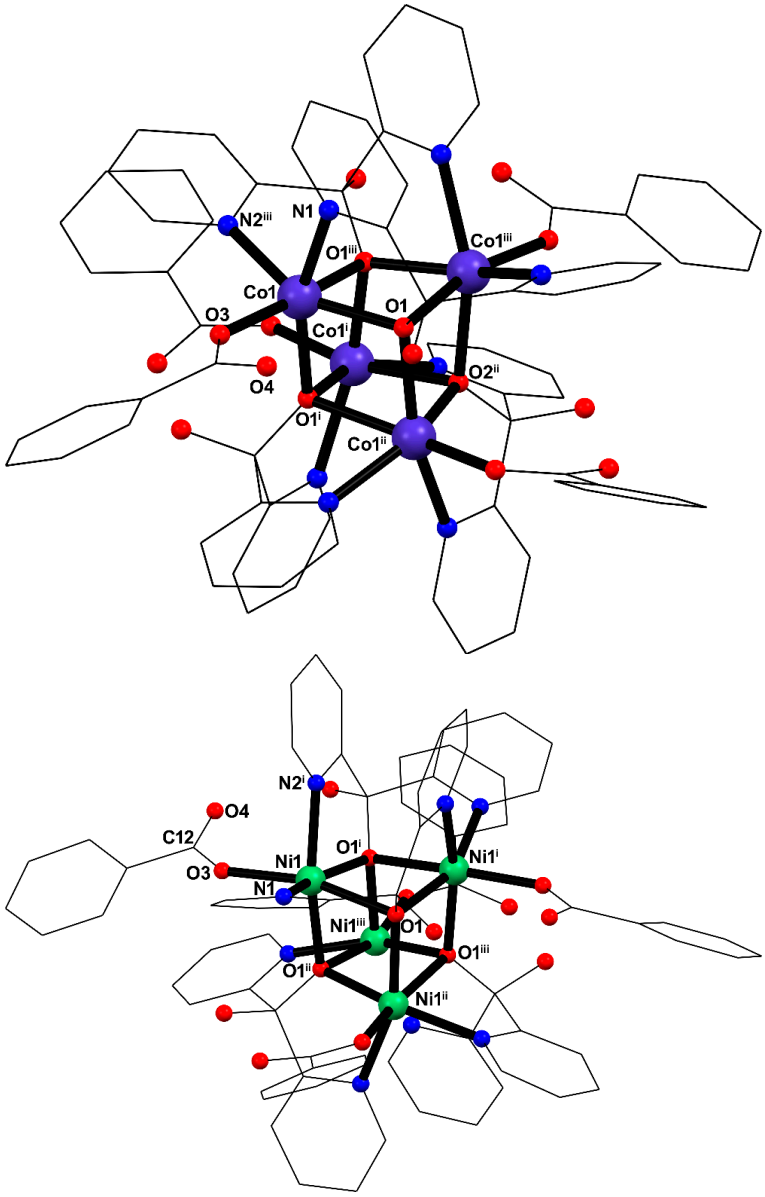

Figure 1. Molecular unit of compounds **1** (**top**) and **2** (**bottom**) with atom numbering. Symmetry operations—for **1**: (i) $3/2 - y, -1/2 + x, 3/2 - z$; (ii) $1/2 + y, 3/2 - x, 3/2 - z$; (iii) $2 - x, 1 - y, +z$; for **2**: (i) $-y, x, 2 - z$; (ii) $y, -x, 2 - z$; (iii) $-x, -y, z$.

Table 2. Selected bond lengths (Å), distances (Å) and bond angles (°) for **1** and **2**.

(1)		(2)	
Co1–O1^{i}	2.111(2)	Ni1–O1^{i}	2.005(4)
Co1–O1	2.032(2)	Ni1–O1	2.079(3)
Co1–O1^{iii}	2.233(3)	Ni1–O1^{ii}	2.166(4)
Co1–O3	2.028(3)	Ni1–O3	2.003(5)
Co1–N1	2.166(3)	Ni1–N1	2.032(6)
Co1–N2^{iii}	2.101(4)	Ni1–N2^{i}	2.088(5)
O1–Co1^{ii}	2.111(2)	O1–Ni1^{i}	2.166(4)
O1–Co1^{iii}	2.233(2)	O1–Ni1^{ii}	2.005(4)
O1–C1	1.395(4)	O1–C1	1.380(7)
C1–O2	1.390(5)	O2–C1	1.389(8)
O4–C12	1.233(6)	O4–C12	1.225(9)
C12–O3	1.258(5)	O3–C12	1.258(9)
Co1···Co1^{i}	3.2175(6)	Ni1···Ni1^{i}	3.089(1)
Co1···Co1^{ii}	3.2337(9)	Ni1···Ni1^{ii}	3.191(1)
Co1···Co1^{iii}	3.2337(9)	Ni1···Ni1^{iii}	3.089(1)
Co1–O1–Co1^{i}	102.61(10)	Ni1–O1–Ni1^{ii}	97.48(16)
Co1^{i}–O1–Co1^{iii}	96.17(9)	Ni1^{i}–O1–Ni1^{ii}	95.47(16)
Co1–O1–Co1^{iii}	97.83(9)	Ni1^{i}–O1–Ni1	102.78(17)

Symmetry operations—for **1**: (i) $3/2 - y, -1/2 + x, 3/2 - z$; (ii) $1/2 + y, 3/2 - x, 3/2 - z$; (iii) $2 - x, 1 - y, +z$; for **2**: (i) $-y, x, 2 - z$; (ii) $y, -x, 2 - z$; (iii) $-x, -y, z$.

Intramolecular hydrogen bonds involving the $\{(py)_2C(OH)O\}^-$ alcohol group (O2) and the O4 atom from the benzoate moiety are present in the cubane-like core of both compounds, with the following geometric parameters for **1**: O2···O4 = 2.636(4) Å and ∠O2–H2···O4 = 167° and for **2**: O2···O4^{ii} = 2.579(7) Å and ∠O2–H2···O4^{ii} = 167° (ii = $y, -x, -z + 2$). Finally, the crystal packing is further stabilized by a series of weak intermolecular interactions of type Csp2–H···Csp2 and Csp2–H···O in both complexes.

3.2. Magnetic Properties

The static magnetic properties of compounds **1** and **2** under the form $\chi_M T$ versus T plots are shown in Figures 2 and 3. Reduced magnetization plots at 2 and 4 K for both compounds were also obtained, with an additional measurement at 8 K for **1**. At room temperature, the $\chi_M T$ values were approximately 11.7 and 4.6 cm^3 K mol^{-1} for **1** and **2**, respectively. These values are slightly higher than the theoretical estimates of 7.5 or 4.4 cm^3 K mol^{-1} expected for four non-interacting Co^{II} (S = 3/2, g = 2.0) or Ni^{II} (S = 1, $g \approx 2.1$) ions. For the Co^{II} case, the deviation and the first observed decrease upon cooling are attributed to first-order spin-orbit coupling (SOC), leading to a g-factor exceeding the free-electron value and the depopulation of higher excited J states, respectively [76]. Later, both compounds exhibited a progressive increase in $\chi_M T$ upon cooling, reaching maxima of 12.4 and 8.7 cm^3 K mol^{-1} at 5.3 K and 7 K for **1** and **2**, respectively. Subsequently, $\chi_M T$ decreased to 11.5 (**1**) and 7.6 (**2**) cm^3 K mol^{-1} at 2.4 and 2.75 K, respectively. No maximum in magnetic susceptibility was observed within the measured temperature range (Figure S2). This behavior suggests the coexistence of ferromagnetic interactions and zfs, typical for Co^{II} and Ni^{II} ions in octahedral ligand fields, or dipolar magnetic couplings between the S = 6 (**1**) or 4 (**2**) ground states of neighboring tetranuclear units. The latter explanation is the most plausible in the case of the Co_4 complex with half-integer local spin momenta. Specifically, a positive axial zfs component (D) for the Ni^{II} ion in **2** could partially explain the low-temperature $\chi_M T$ decay, as it would result in a non-magnetic M_S ground state. For **2**, the magnetization value at 2 K and 60 kOe (7.4 μB) is lower than the expected saturation value of ≈ 8.4 μ_B for an S = 4 ground state with g = 2.1. Furthermore,

the non-superposition of the M-versus-H/T plots (insets in Figures 2 and 3) indicates strong magnetic anisotropy and magnetic couplings. While the reduced magnetization curves of **1** are not expected to superimpose due to the known zfs in octahedral cobalt(II) complexes, the expected effect should be less pronounced due to the large D value typical of such systems. Therefore, the observed magnetic susceptibility behavior of **1** suggests the presence of magnetic interactions on the order of several cm^{-1} between the Co^{II} ions. The magnetic behavior of compounds **1** and **2** is intricate, primarily due to the interplay of first-order SOC or zfs with both intra- ferro- and antiferromagnetic interactions and possible additional intermolecular antiferromagnetic interactions. Although the four M^{II} ions in these compounds are crystallographically equivalent, the molecular symmetry leads to a spin topology that includes multiple magnetic coupling pathways, complicating the analysis.

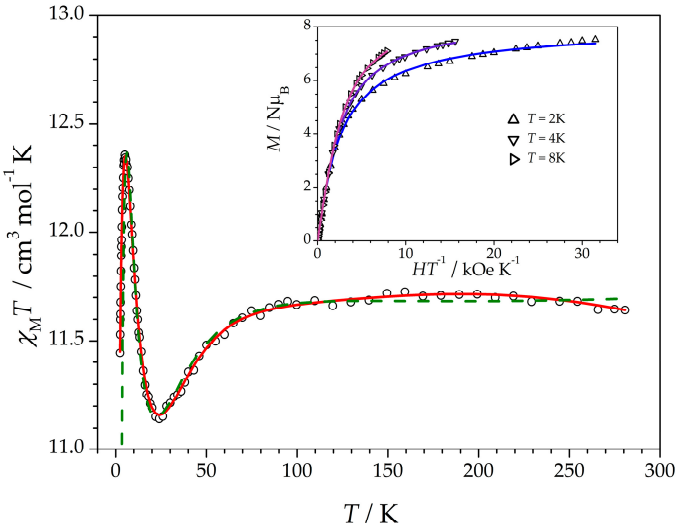

Figure 2. Temperature dependence of $\chi_M T$ (empty circles) for compound **1**. Solid and dashed lines represent the best-fit curves (see text) obtained using a model incorporating SOC (red line, Equation (2)) or zfs (green line, Equation (6)) applied to Co^{II} ions, combined with an exchange-coupling Hamiltonian (Equation (3)). Inset: isothermal reduced magnetization curves (empty triangles) for **1** (solid lines are visual guides).

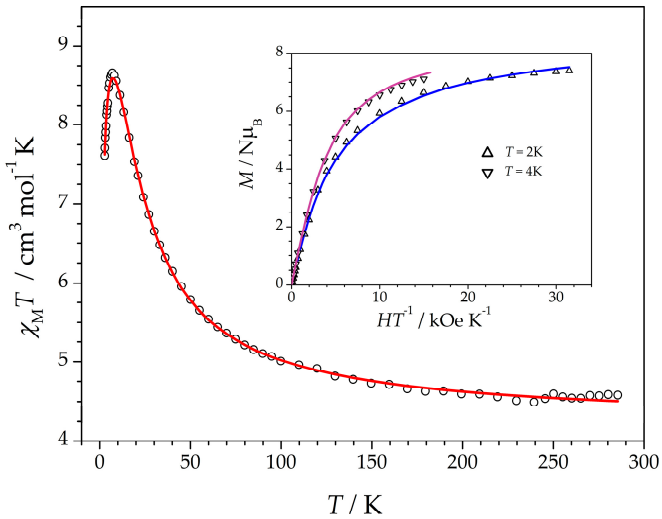

Figure 3. Temperature dependence of $\chi_M T$ (empty circles) for compound **2**. Inset: isothermal reduced magnetization curves (empty triangles). Solid lines represent the best-fit curves (see text) obtained using a model incorporating zfs (Equation (6)) applied to Ni^{II} ions, combined with an exchange-coupling Hamiltonian (Equation (3)).

While simplified models offer some preliminary insights, a comprehensive theoretical study is necessary to quantify these magnetic parameters accurately. The presence of two distinct intramolecular M···M distances in the crystal structure implies the existence of at least two different magnetic coupling constants J_i (Figure 4), which are mediated by two oxygen atoms from the alkoxo groups within the M–O–M exchange pathway, forming a M_2O_2 magnetic unit. As mentioned earlier, previous studies have highlighted the strong dependence of the magnitude and nature of these interactions on the M–O–M angle (α, Figure 5) [19,31,32,59,77,78]. Specifically, α values below a critical "magic angle" favor ferromagnetic coupling, whereas larger angles promote antiferromagnetic interactions. This critical angle is also influenced by the specific metal ion involved, as observed in bis-μ-azido or bis-μ-thiocyanate dinuclear complexes [58]. While well established in copper(II) or nickel(II) dinuclear compounds, the correlation is more nuanced in cobalt(II) systems due to the additional magnetic orbitals involved, including one of t_{2g} symmetry. Nevertheless, recent studies have indicated a tendency toward stronger ferromagnetic interactions in cobalt(II) complexes for smaller α values, consistent with observations in other transition metal complexes [78,79]. Furthermore, the M_2O_2 coupling units in these systems can be symmetrical or asymmetrical with one or two different α angles, respectively, adding another layer of complexity to the magnetic analysis. Other geometric distortions, such as the butterfly distortion of the M_2O_2 unit described by the δ angle (Figure 5), can affect the magnetic coupling, though in compounds **1** and **2**, this distortion is only moderate (Table 3). In dinuclear complexes, α and γ (the angle describing the deviation of the O–R bond from the M_2O plane) are often correlated due to the inherent geometric flexibility of the system [76,77]. However, in M_4O_4 cubane structures, some of the OR bridging groups connect more than two metal ions (μ_3-OR), imposing a specific γ angle and preventing a direct correlation between δ or γ and α [79].

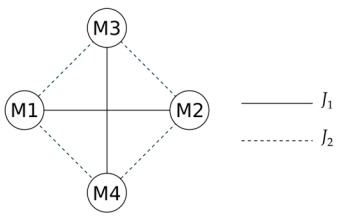

Figure 4. Schematic view of the topology of the spin coupling in **1** and **2**. The numbering system for the metal centers in this scheme is the one used in the definition of the Hamiltonians described in the text, and it relates to the structural labels as M1 = Co1; M2 = $Co1^{iii}$; M3 = $Co1^{i}$, M4 = $Co1^{ii}$ for **1** and M1 = Ni1, M2 = $Ni1^{i}$, M3 = $Ni1^{iii}$, M4 = $Ni1^{ii}$ for **2**.

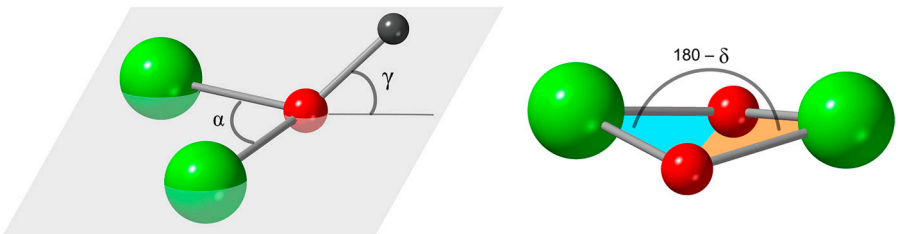

Figure 5. Depiction of structural parameters of the $M_2(OR)_2$ core tuning the magnetic couplings in **1** and **2**. Color codes: green, metal; red, oxygen; and gray, carbon.

Table 3. Most relevant structural parameters and DFT-calculated exchange-coupling constants (J) for the magnetic exchange pathways in **1** and **2**.

	1		**2**	
	J_1	J_2	J_1	J_2
$d_{M...M}$ [a]	3.217	3.234	3.089	3.191
$d_{M...O}$ [a]	2.032; 2.233	2.032; 2.111	2.006; 2.166	2.166; 2.079
α [b]	97.8; 97.8	102.6; 96.2	95.5; 95.5	102.8; 97.5
δ [b]	14.5	11.0	19.0	8.3
γ [b]	39.1; 39.1	57.7; 46.8	35.3; 35.3	48.6; 60.8
J_{DFT} [c]	+0.3	+2.6	+14.6	+3.2
J_{Fit} [c]	+0.12/−0.6	+3.4/+4.8	+14.5/+15.1	+2.3/+2.4

[a] In Å. [b] In degrees. [c] In cm^{-1}.

To streamline the computational estimation of magnetic coupling constants in **1** and **2**, a strategic simplification was employed: two Ni^{II} or Co^{II} ions in the tetranuclear complex were replaced with diamagnetic Zn^{II} ions, maintaining the experimental geometry of the system. This substitution ensures that only two paramagnetic ions are involved in each magnetic coupling interaction at a time, significantly reducing the complexity of the calculations. Importantly, this approach preserves the electron configuration of the system and avoids electronic artifacts that could arise from geometric truncation or the construction of oversimplified models. The nature and magnitude of J for the two systems were estimated using the broken-symmetry approximation, a well-established method described in prior studies. The results, summarized in Table 3, reveal that the magnetic interactions in both systems are predominantly ferromagnetic. Furthermore, the strength of these interactions is inversely correlated with the α angle for **2**, with lower α values corresponding to stronger ferromagnetic coupling, aligning with previously established correlations in the literature, mainly with those results found for similar M_4 cubanes [19,31,32]. It is worth noting that while the magnetic coupling constants (J_1 and J_2) in compound **1** generally agree with the predicted values from a previous correlation in Co_4 truncated dicubanes [79], some discrepancies exist. The observed J_1 value is lower than expected, likely due to one of the M–O bond lengths being significantly longer than usual, which can weaken the magnetic interaction (Table 3). However, it is important to remember that other geometric parameters can also influence the strength and nature of magnetic couplings. The interplay of these factors should be considered for a more in-depth analysis of the magnetic behavior of this compound.

A further contributing factor to the magnetic behavior of compounds **1** and **2** is the zfs tensor. This tensor is characterized by two components: an axial (D) and an equatorial (E) component, with their ratio (E/D) representing the rhombicity. These parameters originate from first-order SOC in Co^{II} and second-order SOC in Ni^{II}, which also determine the g-factor components of these ions. To evaluate these parameters for M^{II} ions, CASSCF calculations were performed on M_4 experimental geometries, wherein diamagnetic Zn^{II} ions replaced three paramagnetic M^{II} ions. The results in Table 4 reveal typical D and g values for cobalt(II) and nickel(II) complexes. The high rhombicity observed is consistent with the significant distortion of the coordination sphere around both metal ions. While CASSCF/NEVPT2 calculations offer a more accurate approach for determining zfs parameters, their computational cost becomes prohibitive when applied to the **MZn_3** models. Therefore, a reasonable approximation involves reducing the system to mononuclear M_1 models. The results obtained from these models must be compared with those from the more extensive **MZn_3** systems at the same calculation level to evaluate the effect of molecular modeling on the electronic structure and its zfs parameters. Two mononuclear models

were employed: one in which the complete coordination sphere ligands were retained (**M_1** model), and another in which the peripheral pyridine or phenyl groups were replaced with methyl groups (**trimmed M_1** model). Given the consistency of results between the simplified mononuclear models and the more complex **MZn_3** system (Table 3), the simplified model is suitable for evaluating zfs parameters, enabling higher-level computational studies. Consequently, CASSCF/NEVPT2 calculations performed on the trimmed M_1 model yielded results comparable to those obtained with simpler, less accurate methodologies, but showing a weaker zfs. This agreement reinforces the reliability of the calculated order of magnitude and sign of D, the magnetic rhombicity (E/D) and the parallel ($g_{||}$) and perpendicular ($g_{\perp}$) components of the g-factor.

Table 4. Calculated zfs parameters, g-factor average (g_{avg}) and perpendicular ($g_{\perp}$) and parallel ($g_{||}$) components for **MZn_3**, **M_1** and **trimmed M_1** models of **1** and **2** derived from CASSCF and CASSCF/NEVPT2 (in parentheses) calculations.

	$CoZn_3$	**Co_1**	**Trimmed Co_1**	**$NiZn_3$**	**Ni_1**	**Trimmed Ni_1**
D [a]	+44.3	+46.5	+44.8 (+34.1)	+7.6	+9.3	+9.3 (+6.8)
E/D	0.216	0.250	0.255 (0.253)	0.080	0.098	0.089 (0.080)
$g_{\|\|}$	2.170	2.175	2.178 (2.089)	2.300	2.291	2.290 (2.206)
$g_{\perp}$	2.666	2.706	2.690 (2.449)	2.358	2.358	2.357 (2.253)
g_{avg}	2.512	2.541	2.531 (2.336)	2.339	2.336	2.335 (2.238)

[a] In cm^{-1}.

Following the conclusions derived from the theoretical study, a rational analysis of the experimental thermal dependence of $\chi_M T$ of **1** was conducted. This analysis initially involved examining the entire temperature range by applying a first-order SOC Hamiltonian ($\hat{H}_{SOC}$) through the T-P isomorphism formalism, as described by Equation (2) [76]. This equation characterizes the coupling between orbital (L) and spin (S) angular momenta. The parameters λ, g_e and α represent the SOC parameter, the electron g-factor and the orbital reduction factor ($\alpha = A\kappa$), respectively. Here, the κ parameter accounts for the reduction in orbital momentum due to electron delocalization, while the A parameter reflects the contribution of the upper $^4T_{1g}(^4P)$ state to the $^4T_{1g}(^4F)$ ground state, with values ranging from 1.5 to 1.0 under weak and strong crystal-field limits. Under axial distortion of the ideal O_h symmetry in the cobalt coordination sphere, the ground triplet level $^4T_{1g}$ splits into the singlet $^4A_2$ and doublet ^4E levels. This splitting, driven by second-order SOC, further generates two and four Kramers doublets, separated by an energy gap defined by the Δ parameter. This model effectively reproduces the magnetic behavior of each Co^{II} ion when isolated. However, to incorporate magnetic couplings between paramagnetic centers via a spin Hamiltonian, it was assumed that these magnetic interactions were sufficiently weak to act primarily when the ground Kramers doublet of each Co^{II} ion was predominantly populated. Although this assumption is not strictly true, it is not far from reality, and therefore, it is unnecessary to use other, more sophisticated methods as we have done in the past. Consequently, each paramagnetic center was treated as an effective spin moment ($S_{eff} = 1/2$) with a temperature-dependent g_{eff}, obtained through the application of the $\hat{H}_{SOC}$ Hamiltonian. Under these assumptions, the magnetic interactions were also considered effective (J_{eff}), related to real interactions by a factor of 25/9 [76]. The exchange-coupling Hamiltonian in Equation (2) is defined based on the spin-interaction topology illustrated in Figure 4. Finally, the dipolar interactions between the ferromagnetic ground states of neighboring Co_4 units were included through θ under a mean-field model via Equation (5). By combining the $\hat{H}_{Exchange}$ and $\hat{H}_{zeem-eff}$ Hamiltonians [Equations (3) and (4)], the best-fit parameters determined using the XVPMag software [68] were $A = 1.29$, $\lambda = -103.3$ cm^{-1}, $\Delta = 454$ cm^{-1}, $J_1 = -0.6$ cm^{-1}, $J_2 = +4.8$ cm^{-1} and $\theta = -0.42$ K. The agreement between

experimental and simulated data was remarkable, as indicated by the agreement factor $F = 7.8 \times 10^{-6}$, defined as $\sum(\chi_M T_{exp} - \chi_M T_{calcd}]^2/\sum(\chi_M T_{exp})^2$.

$$\hat{H}_{SOC} = -\alpha\lambda\hat{L}\cdot\hat{S} + \Delta\left[\hat{L}_z^2 - \frac{1}{3}L(L+1)\right] + \beta H\left[g_e\hat{S} - \alpha\hat{L}\right] \quad (2)$$

$$\hat{H}_{Exchange} = -J_1\left(\hat{S}_{M1}\cdot\hat{S}_{M2} + \hat{S}_{M3}\cdot\hat{S}_{M4}\right) - J_2\left(\hat{S}_{M1}\cdot\hat{S}_{M3} + \hat{S}_{M1}\cdot\hat{S}_{M4} + \hat{S}_{M2}\cdot\hat{S}_{M3} + \hat{S}_{M2}\cdot\hat{S}_{M4}\right) \quad (3)$$

$$\hat{H}_{zeem-eff} = g_{eff}\beta H\sum_{i=1}^{4}\hat{S}_{Co_i} \quad (4)$$

$$\chi_M T_{exp} = \chi_M T_{M_4} \times T/(T-\theta) \quad (5)$$

Further refinement was undertaken by incorporating second-order SOC, which explicitly accounts for the zfs experienced by the local $S = 3/2$ ground state of each Co^{II} ion, as described by Equation (6), where D represents the axial magnetic component of the zfs. A temperature-independent paramagnetism (TIP) term was introduced in the model to address the depopulation of the higher-energy Kramers doublet occurring at elevated temperatures. In order to minimize overparameterization, the zfs rhombic magnetic component (E) was considered null. As before, the dipolar magnetic interaction along the crystal lattice between neighboring Co_4 units was also considered. The combined model, incorporating zfs (Equation 6), exchange (Equation (2)) and Zeeman Hamiltonians (Equation (7)), yielded an excellent fit to the experimental data, as evidenced by the agreement factor $F = 6.6 \times 10^{-5}$. The best-fit parameters obtained were $g = 2.450$, $D = +58.1$ cm^{-1}, $J_1 = +0.12$ cm^{-1}, $J_2 = +3.40$ cm^{-1}, TIP = 797.1×10^{-6} cm^3 mol^{-1} and $\theta = -1.8$ K. The large positive D value obtained is consistent with those reported in the literature for other octahedral high-spin cobalt(II) complexes. However, it is slightly higher than the local D values derived from theoretical calculations (Table 4), even if the local zfs tensors are not aligned (Figure S3). Despite some minor discrepancies, this correspondence further validates the employed model and highlights the accuracy of both the experimental and theoretical approaches in describing the magnetic behavior of the cobalt(II) complex.

$$\hat{H}_{zfs} = D\sum_{i=1}^{4}\left[\hat{S}_{z,i}^2 - \frac{1}{3}S_i(S_i+1)\right] \quad (6)$$

$$\hat{H}_{Zeem} = g\beta H\sum_{i=1}^{4}\hat{S}_{M_i} \quad (7)$$

The situation is more straightforward for compound **2**. In this case, the corresponding Hamiltonian is given by the sum of terms $\hat{H}_{Exchange} + \hat{H}_{zfs} + \hat{H}_{Zeem}$ (Equations (3), (5) and (6)). Typically, the most frequently adopted approach involves assuming that the local z axes are collinear and, consequently, parallel to the S_4 axis in this context [32,33]. In some reported cases, taking into account the distortions in the coordination environment of the nickel atoms, it has been deemed more appropriate to assume that the local anisotropy axes are orthogonal to the S_4 axis [21,25,80,81]. However, in our case, the distortion of the octahedral geometry is significant enough that it precludes a priori confidence in selecting the most suitable canting angle between z and S_4. In fact, CASSCF calculations have revealed a canting angle of 67.7° in this compound. Therefore, we decided to investigate the effect on the quality of the simultaneous magnetization and susceptibility fit when the canting angle (β) is varied between 0 and 90 degrees for positive starting D values. The results, obtained using the PHI package [74], are presented in Figure 6, which shows the optimal outcomes in terms of lower error residuals R ($R = [\sum(\chi_{Mexp} - \chi_{Mcalcd})^2][\sum(M_{exp} - M_{calcd})^2]$. The

best fits to the experimental data are attained with two distinct sets of values, as detailed in Table 5, corresponding to β angles of 43 and 69°. An excellent fit was achieved without accounting for possible intermolecular interactions. No improvement was observed when an E parameter was included to account for potential rhombic distortion of the Ni^{II} ions. Remarkably, the values of J_1, J_2, D and β determined through the fitting procedure are in close agreement with those derived from computational calculations.

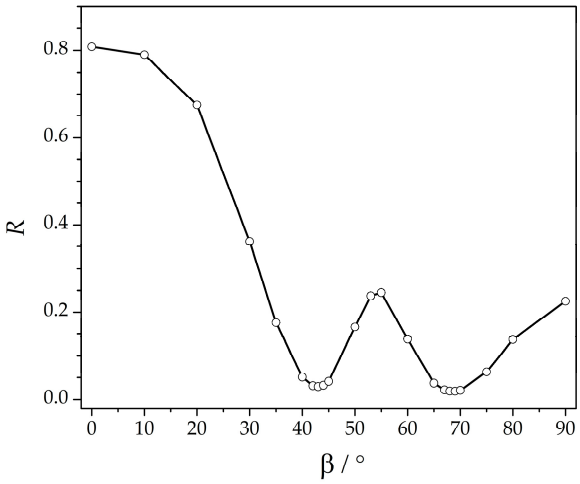

Figure 6. Residual error in the simultaneous fitting of $\chi_M T$ and M for different values of the β angle and $D > 0$ for compound **2**.

Table 5. Best-fit parameters obtained for complex **2** (see text).

Parameters	Fit	
β [a]	43	69
J_1 [b]	15.1(2)	14.5(2)
J_2 [b]	2.42(2)	2.34(2)
D [b]	11.76(3)	10.44(3)
g	2.050(1)	2.056(1)
R	0.02966	0.01952

[a] In degrees. [b] In cm^{-1}.

4. Conclusions

New tetranuclear complexes $[M_4\{(py)_2C(OH)O\}_4(O_2CPh)_4]$ (M = Co, Ni) were synthesized by reacting $M(NO_3)_2{\cdot}6H_2O$, di-2-pyridyl ketone and sodium benzoate in methanol. X-ray crystallography revealed that compounds **1** and **2** feature a cubane-like $[M_4O_4]$ core with S_4 symmetry. Experimental magnetic data analyses for the nickel compound, conducted using simultaneous $\chi_M(T)$ and $M(H,T)$ fitting, confirmed ferromagnetic interactions among the four Ni ions in the cubane cluster, resulting in an $S = 4$ ground state. The obtained exchange-coupling J values correlate well with previously established magnetostructural relationships, where stronger ferromagnetic coupling is associated with a smaller Ni–O–Ni angle. The analysis also indicated significant zfs ($D = +10 - 12$ cm^{-1}) and enabled the assessment of local anisotropy axes orientation.

For the cobalt complex, the high magnetic anisotropy was analyzed using two different models for the fitting procedures, considering first-order SOC through *T-P* isomorphism formalism or local zfs effects. In both approaches, predominant ferromagnetic intracluster interactions were observed, yielding an $S = 6$ ground state. In contrast to the Ni compound, a low negative J value was observed for the smallest Co–O–Co angle, suggesting that additional structural factors influence Co···Co interactions.

Theoretical calculations, including DFT and CASSCF/NEVPT2 methods, provided valuable insights into the magnetic coupling constants and zfs parameters, aiding in the fitting processes. The remarkable agreement between experimental data and theoretical models highlights the reliability of the methodologies employed. In highly complex systems such as these, computational approaches have once again proven to be essential tools for conducting comprehensive analyses of experimental results.

Supplementary Materials: The following supporting information can be downloaded at: https://www.mdpi.com/article/10.3390/magnetochemistry11040034/s1, Figure S1: Asymmetric units; Figure S2: Magnetic susceptibility versus *T* curves; Figure S3: Orientation of the calculated local *D* tensors.

Author Contributions: Conceptualization, M.G.F.V. and R.G.; investigation, C.P. and C.R.-D.; crystallography, G.P.G. and M.G.F.V.; magnetic study and analysis, C.P., J.C., M.A.N., R.C. and R.G.; theoretical calculations, S.V. and J.C.; formal analysis, J.C., R.C. and R.G.; resources, M.A.N., J.C., M.G.F.V. and R.G.; writing—original draft preparation, G.P.G., J.C., R.C. and R.G.; writing—review and editing, R.C. and R.G.; visualization, G.P.G. and R.C.; supervision, M.G.F.V. and R.G.; funding acquisition, J.C., G.P.G., M.G.F.V. and R.G. All authors have read and agreed to the published version of the manuscript.

Funding: Financial support from the Comisión Sectorial de Investigación Científica (Uruguay, Project 453), Agencia Nacional de Investigación e Innovación (Uruguay, FCE_1_2021_1_167507) and PEDECIBA is gratefully acknowledged. G.P.G., M.G.F.V. and M.A.N thank the Brazilian agencies FAPERJ and CNPq for financial support. C.P. thanks Agencia Nacional de Investigación e Innovación and S.V thanks Comisión Académica de Posgrado (Universidad de la República) for graduate scholarships.

Institutional Review Board Statement: Not applicable.

Informed Consent Statement: Not applicable.

Data Availability Statement: The original contributions presented in this study are included in the article and Supplementary Materials. Further inquiries can be directed to the corresponding authors.

Acknowledgments: We thank LABCri-UFMG and LDRX-UFF for crystallographic facility access.

Conflicts of Interest: The authors declare no conflicts of interest.

References

1. Sessoli, R.; Gatteschi, D.; Caneschi, A.; Novak, M. Magnetic bistability in a metal-ion cluster. *Nature* **1993**, *365*, 141–143. [CrossRef]
2. Aromí, G.; Brechin, E.K. Synthesis of 3*d* Metallic Single-Molecule Magnets. In *Single-Molecule Magnets and Related Phenomena*; Winpenny, R., Ed.; Springer: Berlin/Heidelberg, Germany, 2006; Volume 122, pp. 1–67.
3. Sessoli, R.; Powell, A.K. Strategies towards single molecule magnets based on lanthanide ions. *Coord. Chem. Rev.* **2009**, *253*, 2328–2341. [CrossRef]
4. Christou, G. Single-molecule magnets: A molecular approach to nanoscale magnetic materials. *Polyhedron* **2005**, *24*, 2065–2075. [CrossRef]
5. Tasiopoulos, A.J.; Vinslava, A.; Wernsdorfer, W.; Abboud, K.A.; Christou, G. Giant Single-Molecule Magnets: A $\{Mn_{84}\}$ Torus and Its Supramolecular Nanotubes. *Angew. Chem. Int. Ed.* **2004**, *43*, 2117–2121. [CrossRef]
6. Manoli, M.; Inglis, R.; Manos, M.J.; Nastopoulos, V.; Wernsdorfer, W.; Brechin, E.K.; Tasiopoulos, A.J. A $[Mn_{32}]$ Double-Decker Wheel. *Angew. Chem. Int. Ed.* **2011**, *50*, 4441–4444. [CrossRef] [PubMed]
7. Powell, G.W.; Lancashire, H.N.; Brechin, E.K.; Collison, D.; Heath, S.L.; Mallah, T.; Wernsdorfer, W. Building Molecular Minerals: All Ferric Pieces of Molecular Magnetite. *Angew. Chem. Int. Ed.* **2004**, *43*, 5772–5775. [CrossRef] [PubMed]
8. Kong, X.J.; Wu, Y.; Long, L.S.; Zheng, L.S.; Zheng, Z. A Chiral 60-Metal Sodalite Cage Featuring 24 Vertex-Sharing $[Er_4(\mu_3\text{-}OH)_4]$ Cubanes. *J. Am. Chem. Soc.* **2009**, *131*, 6918–6919. [CrossRef]
9. Wang, W.G.; Zhou, A.J.; Zhang, W.X.; Tong, M.L.; Chen, X.M.; Nakano, M.; Beedle, C.C.; Hendrickson, D.N. Giant Heterometallic $Cu_{17}Mn_{28}$ Cluster with T_d Symmetry and High-Spin Ground State. *J. Am. Chem. Soc.* **2007**, *129*, 1014–1015. [CrossRef]
10. Liu, T.; Zhang, Y.J.; Wang, Z.M.; Gao, S. A 64-Nuclear Cubic Cage Incorporating Propeller-like Fe^{III}_8 Apices and $HCOO^-$ Edges. *J. Am. Chem. Soc.* **2008**, *130*, 10500–10501. [CrossRef]

11. Zhang, Z.M.; Yao, S.; Li, Y.G.; Clerac, R.; Lu, Y.; Su, Z.M.; Wang, E.B. Protein-Sized Chiral Fe_{168} Cages with NbO^{-} Type Topology. *J. Am. Chem. Soc.* **2009**, *131*, 14600–14601. [CrossRef]
12. Müller, A.; Krickemeyer, E.; Das, S.K.; Kögerler, P.; Sarkar, S.; Bögge, H.; Schmidtmann, M.; Sarkar, S. Linking Icosahedral, Strong Molecular Magnets {Mo} to Layers—A Solid-State Reaction at Room Temperature. *Angew. Chem. Int. Ed.* **2000**, *39*, 1612–1614. [CrossRef]
13. Moushi, E.E.; Lampropoulos, C.; Wernsdorfer, W.; Nastopoulos, V.; Christou, G.; Tasiopoulos, A.J. Inducing Single-Molecule Magnetism in a Family of Loop-of-Loops Aggregates: Heterometallic $Mn_{40}Na_4$ Clusters and the Homometallic Mn_{44} Analogue. *J. Am. Chem. Soc.* **2010**, *132*, 16146–16155. [CrossRef] [PubMed]
14. Kong, J.; Ren, Y.P.; Chen, W.X.; Long, L.S.; Zheng, Z.; Huang, R.B.; Zheng, L.S. A Four-Shell, Nesting Doll-like 3*d*–4*f* Cluster Containing 108 Metal Ions. *Angew. Chem. Int. Ed.* **2008**, *47*, 2398–2401. [CrossRef] [PubMed]
15. Moushi, E.E.; Lampropoulos, C.; Wernsdorfer, W.; Nastopoulos, V.; Christou, G.; Tasiopoulos, A. A Large $[Mn_{10}Na]_4$ Loop of Four Linked Mn_{10} Loops. *J. Inorg. Chem.* **2007**, *46*, 3795–3797. [CrossRef] [PubMed]
16. Stamatatos, T.C.; Abboud, K.A.; Wernsdorfer, W.; Christou, G. "Spin Tweaking" of a High-Spin Molecule: An Mn_{25} Single-Molecule Magnet with an S=61/2 Ground State. *Angew. Chem. Int. Ed.* **2007**, *46*, 884–888. [CrossRef]
17. Ponomaryov, A.N.; Kim, N.; Hwang, J.; Nojiri, H.; Van Tol, J.; Ozarowski, A.; Park, J.; Jang, Z.; Suh, B.; Yoon, S.; et al. Structural Tailoring Effects on the Magnetic Behavior of Symmetric and Asymmetric Cubane-Type Ni Complexes. *Chem. Asian J.* **2013**, *8*, 1152–1159. [CrossRef]
18. Aromí, G.; Bouwman, E.; Burzurí, E.; Carbonera, C.; Krzystek, J.; Luis, F.; Schlegel, C.; Van Slageren, J.; Tanase, S.; Teat, S.J. A Novel Ni_4 Complex Exhibiting Microsecond Quantum Tunneling of the Magnetization. *Chem. Eur. J.* **2008**, *14*, 11158–11166. [CrossRef]
19. Herchel, R.; Nemec, I.; Machata, M.; Trávníček, Z. Solvent- Induced Structural Diversity in Tetranuclear Ni (II) Schiff-Base Complexes: The First Ni_4 Single-Molecule Magnet with a Defective Dicubane-like Topology. *Dalton Trans.* **2016**, *45*, 18622–18634. [CrossRef]
20. Ferguson, A.; Lawrence, J.; Parkin, A.; Sanchez-Benitez, J.; Kamenev, K.V.; Brechin, E.K.; Wernsdorfer, W.; Hill, S.; Murrie, M. Synthesis and Characterisation of a Ni_4 Single-Molecule Magnet with S_4 Symmetry. *Dalton Trans.* **2008**, *45*, 6409–6414. [CrossRef]
21. Escobar, L.B.L.; Guedes, G.P.; Soriano, S.; Marbey, J.; Hill, S.; Novak, M.A.; Vaz, M.G.F. Synthesis, Magnetic and High-Field EPR Investigation of Two Tetranuclear Ni^{II}-Based Complexes. *Inorg. Chem.* **2019**, *58*, 14420–14428. [CrossRef]
22. Yang, E.-C.; Wernsdorfer, W.; Hill, S.; Edwards, R.S.; Nakano, M.; Maccagnano, S.; Zakharov, L.N.; Rheingold, A.L.; Christou, G.; Hendrickson, D.N. Exchange bias in Ni_4 single-molecule magnets. *Polyhedron* **2003**, *22*, 1727–1733. [CrossRef]
23. Yang, E.-C.; Wernsdorfer, W.; Zakharov, L.N.; Karaki, Y.; Yamaguchi, A.; Isidro, R.M.; Lu, G.D.; Wilson, S.A.; Rheingold, A.L.; Ishimoto, H.; et al. Fast Magnetization Tunneling in Tetranickel (II) Single-Molecule Magnets. *Inorg. Chem.* **2006**, *45*, 529–546. [CrossRef]
24. Moragues-Canovas, M.; Helliwell, M.; Ricard, L.; Riviere, E.; Wernsdorfer, W.; Brechin, E.; Mallah, T. An Ni_4 Single-Molecule Magnet: Synthesis, Structure and Low-Temperature Magnetic Behavior. *Eur. J. Inorg. Chem.* **2004**, *2004*, 2219–2222. [CrossRef]
25. Guedes, G.P.; Soriano, S.; Comerlato, N.M.; Speziali, N.L.; Lahti, P.M.; Novak, M.A.; Vaz, M.G.F. Two cobalt (II) cubane compounds: The key role of small ligand changes on the crystal packing and magnetic properties. *Eur. J. Inorg.* **2012**, *2012*, 5642–5648. [CrossRef]
26. Yang, E.-C.; Hendrickson, D.N.; Wernsdorfer, W.; Nakano, M.; Zakharov, L.N.; Sommer, R.D.; Rheingold, A.L.; Ledezma-Gairaud, M.; Christou, G. Cobalt single-molecule magnet. *J. Appl. Phys.* **2002**, *91*, 7382–7384. [CrossRef]
27. Zhang, S.-H.; Zhang, Y.D.; Zou, H.H.; Guo, J.J.; Li, H.P.; Song, Y.; Liang, H. A family of cubane cobalt and nickel clusters: Syntheses, structures and magnetic properties. *Inorg. Chim. Acta* **2013**, *396*, 119–125. [CrossRef]
28. Ma, X.-F.; Wang, Z.; Chen, X.-L.; Kurmoo, M.; Zeng, M.-H. Ligand effect on the single-molecule magnetism of tetranuclear Co (II) cubane. *Inorg. Chem.* **2017**, *56*, 15178–15186. [CrossRef]
29. Wu, Y.; Xi, J.; Xiao, T.; Ferrando-Soria, J.; Ouyang, Z.; Wang, Z.; Luo, S.; Liu, X.; Pardo, E. Switching of easy-axis to easy-plane anisotropy in cobalt (II) complexes. *Inorg. Chem. Front.* **2021**, *8*, 5158–5168. [CrossRef]
30. Galloway, K.W.; Whyte, A.M.; Wernsdorfer, W.; Sanchez-Benitez, J.; Kamenev, K.V.; Parkin, A.; Peacock, R.D.; Murrie, M. Cobalt (II) Citrate Cubane Single-Molecule Magnet. *Inorg. Chem.* **2008**, *47*, 7438–7442. [CrossRef]
31. Palacios, M.A.; Mota, A.J.; Perea-Buceta, J.E.; White, F.J.; Brechin, E.K.; Colacio, E. Antiferromagnetic versus Ferromagnetic Exchange Interactions in Bis(μ-$O_{oximate}$) dinickel (II) Units for a Series of Closely Related Cube Shaped Carboxamideoximate-Bridged Ni_4 Complexes. A Combined Experimental and Theoretical Magneto-Structural Study. *Inorg. Chem.* **2010**, *49*, 10156–10165. [CrossRef]
32. Das, A.; Klinke, F.J.; Demeshko, S.; Meyer, S.; Dechert, S.; Meyer, F. Reversible Solvatomagnetic Effect in Novel Tetranuclear Cubane-Type Ni_4 Complexes and Magnetostructural Correlations for the $[Ni_4(\mu_3\text{-}O)_4]$ Core. *Inorg. Chem.* **2012**, *51*, 8141–8149. [CrossRef] [PubMed]

33. Aryaeifar, M.; Rudbari, H.A.; Moreno-Pineda, E.; Cuevas-Vicario, J.V.; Paul, S.; Schulze, M.; Wernsdorfer, W.; Lloret, F.; Moinii, N.; Blacque, O. Synthesis, characterization and magnetic properties of halogenated tetranuclear cubane-like nickel(II) complexes. *New J. Chem.* **2024**, *48*, 3603–3613. [CrossRef]
34. Zaleski, C.M.; Depperman, E.C.; Dendrinou-Samara, C.; Alexiou, M.; Kampf, J.W.; Kessissoglou, D.; Kirk, M.L.; Pecoraro, V.L. Metallacryptate Single-Molecule Magnets: Effect of Lower Molecular Symmetry on Blocking Temperature. *J. Am. Chem. Soc.* **2005**, *127*, 12862–12872. [CrossRef] [PubMed]
35. Papaefstathiou, G.S.; Perlepes, S.P. Families of Polynuclear Manganese, Cobalt, Nickel and Copper Complexes Stabilized by Various Forms of Di-2-pyridyl Ketone. *Comments Inorg. Chem.* **2002**, *23*, 249–274. [CrossRef]
36. Efthymiou, C.G.; Mylonas-Margaritis, I.; Raptopoulou, C.P.; Psycharis, V.; Escuer, A.; Papatriantafyllopoulou, C.; Perlepes, S.P. A Ni11 Coordination Cluster from the Use of the Di-2-Pyridyl Ketone/Acetate Ligand Combination: Synthetic, Structural and Magnetic Studies. *Magnetochemistry* **2016**, *2*, 30. [CrossRef]
37. Tsohos, A.; Dionyssopoulou, S.; Raptopoulou, C.P.; Terzis, A.; Bakalbassis, E.G.; Perlepes, S.P. The gem-Diol Form of $(py)_2$ CO as a Ligand in Cobalt(II) Carboxylate Clusters: A Cubane Complex and a Novel Nonanuclear Species with a Vertex-Sharing Double Square Pyramidal Structure. *Angew. Chem. Int. Ed.* **1999**, *38*, 983–985. [CrossRef]
38. Efthymiou, C.G.; Raptopoulou, C.P.; Terzis, A.; Boča, R.; Korabic, M.; Mrozinski, J.; Perlepes, S.P.; Bakalbassis, E.G. A Systematic Exploration of Nickel(II)/Acetate/Di-2-pyridyl Ketone Chemistry: Neutral and Cationic Clusters, and a Novel Mononuclear Complex. *Eur. J. Inorg. Chem.* **2006**, *2016*, 2236–2252. [CrossRef]
39. Tong, M.-L.; Zheng, S.-L.; Shi, J.-X.; Tong, Y.-X.; Lee, H.K.; Chen, X.-M. Synthesis, crystal structures and properties of six cubane-like transition metal complexes of di-2-pyridyl ketone in gem-diol form. *J. Chem. Soc. Dalton Trans.* **2002**, *2002*, 1727–1734. [CrossRef]
40. Papaefstathiou, G.S.; Escuer, A.; Mautner, F.A.; Raptopoulou, C.; Terzis, A.; Perlepes, S.P.; Vicente, R. Use of the Di-2-pyridyl Ketone/Acetate/Dicyanamide "Blend" in Manganese (II), Cobalt (II) and Nickel (II) Chemistry: Neutral Cubane Complexes. *Eur. J. Inorg. Chem.* **2005**, *2005*, 879–893. [CrossRef]
41. Papatriantafyllopoulou, C.; Efthymiou, C.G.; Raptopoulou, C.P.; Vicente, R.; Manessi-Zoupa, E.; Psycharis, V.; Escuer, A.; Perlepes, S.P. Initial use of the di-2-pyridyl ketone/sulfate "blend" in 3*d*-metal cluster chemistry: Preparation, X-ray structures and physical studies of zinc (II) and nickel (II) cubanes. *J. Mol. Struct.* **2007**, *829*, 176–188. [CrossRef]
42. Wang, H.-S.; Song, Y. Conversion of tetranuclear Ni complexes from a defect dicubane core to a $[Ni_4O_4]$ cubane-like core via addition of 2-hydroxymethylpyridine: Synthesis, crystal structures, and magnetic properties. *Inorg. Chem. Commun.* **2013**, *35*, 86–88. [CrossRef]
43. Katsenis, A.D.; Inglis, R.; Slawin, A.M.Z.; Kessler, V.G.; Brechin, E.K.; Papaefstathiou, G.S. Transforming the cube: A tetranuclear cobalt(II) cubane cluster and its transformation to a dimer of dimers. *Cryst. Eng. Comm.* **2009**, *11*, 2117–2120. [CrossRef]
44. Padhi, S.K.; Sahu, R. Co (II/III) coordinated pyridine alcoholate ligand generated through metal assisted nucleophilic addition to a C=O function: Temperature dependent synthesis of a mononuclear complex and a neutral cubane cluster. *Polyhedron* **2008**, *27*, 2662–2666. [CrossRef]
45. *CRYSALISPRO*; Version 1.171.33.55, release 5 January 2010; CrysAlis171.NET; Oxford Diffraction Ltd.: Abingdon, UK, 2010.
46. Sheldrick, G.M. A short history of SHELX. *Acta Cryst. A* **2008**, *64*, 112–122. [CrossRef]
47. Sheldrick, G.M. *SADABS, Program for Empirical Absorption Correction of Area Detector Data*; University of Göttingen: Göttingen, Germany, 1996.
48. Duisenberg, A.J.M. Indexing in single-crystal diffractometry with an obstinate list of reflections. *J. Appl. Crystallogr.* **1992**, *25*, 92–96. [CrossRef]
49. Duisenberg, A.J.M.; Kroon-Batenburg, L.M.J.; Schreurs, A.M.M. An intensity evaluation method: EVAL-14. *J. Appl. Crystallogr.* **2003**, *36*, 220–229. [CrossRef]
50. Neese, F. Software update: The ORCA program system—Version 5.0. *Wiley Interdiscip. Rev. Comput. Mol. Sci.* **2022**, *12*, e1606. [CrossRef]
51. Weigend, F.; Ahlrichs, R. Balanced basis sets of split valence, triple zeta valence and quadruple zeta valence quality for H to Rn: Design and assessment of accuracy. *Phys. Chem. Chem. Phys.* **2005**, *7*, 3297–3305. [CrossRef]
52. Becke, A.D. Density-functional exchange-energy approximation with correct asymptotic behavior. *Phys. Rev. A* **1988**, *38*, 3098–3100. [CrossRef]
53. Lee, C.; Yang, W.; Parr, R.G. Development of the Colle-Salvetti correlation-energy formula into a functional of the electron density. *Phys. Rev. B* **1988**, *37*, 785–789. [CrossRef]
54. Izsák, R.; Hansen, A.; Neese, F. The resolution of identity and chain of spheres approximations for the LPNO-CCSD singles Fock term. *J. Chem. Phys.* **2012**, *110*, 2413–2417. [CrossRef]
55. Weigend, F. Accurate Coulomb-fitting basis sets for H to Rn. *Phys. Chem. Chem. Phys.* **2006**, *8*, 1057–1065. [CrossRef]
56. Tomasi, J.; Mennucci, B.; Cammi, R. Quantum Mechanical Continuum Solvation Models. *Chem. Rev.* **2005**, *105*, 2999–3094. [CrossRef]

57. Ruiz, E.; Rodríguez-Fortea, A.; Cano, J.; Alvarez, S.; Alemany, P. About the calculation of exchange coupling constants in polynuclear transition metal complexes. *J. Comput. Chem.* **2003**, *24*, 982–989. [CrossRef]
58. Ruiz, E.; Cano, J.; Alvarez, S.; Alemany, P. Magnetic Coupling in End-On Azido-Bridged Transition Metal Complexes: A Density Functional Study. *J. Am. Chem. Soc.* **1998**, *120*, 11122–11129. [CrossRef]
59. Ruiz, E.; Alemany, P.; Alvarez, S.; Cano, J. Toward the Prediction of Magnetic Coupling in Molecular Systems: Hydroxo- and Alkoxo-Bridged Cu(II) Binuclear Complexes. *J. Am. Chem. Soc.* **1997**, *119*, 1297–1303. [CrossRef]
60. Ruiz, E.; Alvarez, S.; Cano, J.; Polo, V. About the calculation of exchange coupling constants using density-functional theory: The role of the self-interaction error. *J. Chem. Phys.* **2005**, *123*, 164110. [CrossRef]
61. Segger, R.; People, J.A. Self-consistent molecular orbital methods. XVIII. Constraints and stability in Hartree–Fock theory. *J. Chem. Phys.* **1977**, *66*, 3045–3050. [CrossRef]
62. Angeli, C.; Cimiraglia, R.; Malrieu, J.P. N-electron valence state perturbation theory: A fast implementation of the strongly contracted variant. *Chem. Phys. Lett.* **2001**, *350*, 297–305. [CrossRef]
63. Angeli, C.; Cimiraglia, R.; Malrieu, J.P. n-electron valence state perturbation theory: A spinless formulation and an efficient implementation of the strongly contracted and of the partially contracted variants. *J. Chem. Phys.* **2002**, *117*, 9138–9153. [CrossRef]
64. Angeli, C.; Cimiraglia, R.; Evangelisti, S.; Leininger, T.; Malrieu, J.-P. Introduction of n-electron valence states for multireference perturbation theory. *J. Chem. Phys.* **2001**, *114*, 10252–10264. [CrossRef]
65. Stoychev, G.L.; Auer, A.A.; Neese, F. Automatic Generation of Auxiliary Basis Sets. *J. Chem. Theory Comput.* **2017**, *13*, 554–562. [CrossRef]
66. Neese, F.; Wenmohs, A.; Hansen, A.; Becker, U. Efficient, approximate and parallel Hartree–Fock and hybrid DFT calculations. A 'chain-of-spheres' algorithm for the Hartree–Fock exchange. *Chem. Phys.* **2009**, *356*, 98–109. [CrossRef]
67. Izsák, R.; Neese, F. An overlap fitted chain of spheres exchange method. *J. Chem. Phys.* **2011**, *135*, 144105. [CrossRef]
68. Cano, J. *XVPMag: X-Virtual Package for Magnetism*; Universidad de Valencia: Valencia, Spain, 2010.
69. Levenberg, K. A method for the solution of certain non-linear problems in least squares. *Q. Appl. Math.* **1944**, *2*, 164–168. [CrossRef]
70. Marquardt, W.D. An Algorithm for Least-Squares Estimation of Nonlinear Parameters. *SIAM J. Appl. Math.* **1963**, *11*, 431–441. [CrossRef]
71. Thomson, J.J. On the structure of the atom: An investigation of the stability and periods of oscillation of a number of corpuscles arranged at equal intervals around the circumference of a circle; with application of the results to the theory of atomic structure. *Lond. Edinb. Dubl. Phil. Mag.* **1904**, *39*, 237–265. [CrossRef]
72. Moscato, P.; Haque, N.M.; Moscato, A. Continued fractions and the Thomson problem. *Sci. Rep.* **2023**, *13*, 7272. [CrossRef]
73. König, E.; Kremer, S. Irreducible tensor operator methods in intermediate-field coupling. *Int. J. Quantum Chem.* **1974**, *8*, 347–362. [CrossRef]
74. Chilton, N.F.; Anderson, R.P.; Turner, L.D.; Soncini, A.; Murray, K.S. PHI: A powerful new program for the analysis of anisotropic monomeric and exchange-coupled polynuclear *d*-and *f*-block complexes. *J. Comput. Chem.* **2013**, *34*, 1164–1175. [CrossRef]
75. Isele, K.; Gigon, F.; Williams, A.F.; Bernardinelli, G.; Franz, P.; Decurtins, S. Synthesis, structure and properties of $\{M_4O_4\}$ cubanes containing nickel (ii) and cobalt (ii). *Dalton Trans.* **2007**, *3*, 332–341. [CrossRef] [PubMed]
76. Lloret, F.; Julve, M.; Cano, J.; Ruiz-García, R.; Pardo, R. Magnetic properties of six-coordinated high-spin cobalt (II) complexes: Theoretical background and its application. *Inorg. Chim. Acta* **2008**, *361*, 3432–3445. [CrossRef]
77. Ruiz, E.; Alemany, P.; Alvarez, S.; Cano, J. Structural Modeling and Magneto-Structural Correlations for Hydroxo-Bridged Copper (II) Binuclear Complexes. *Inorg. Chem.* **1997**, *36*, 3683–3688. [CrossRef]
78. Song, X.; Xue, X. Study on the Magneto-Structural Correlation of a New Dinuclear Cobalt (II) Complex with Double μ-Phenoxo Bridges. *ACS Omega* **2020**, *5*, 8347–8354. [CrossRef]
79. Kant, S.; Saha, S.; Lloret, F.; Cano, J.; Mukherjee, R. A tetracobalt (II) cluster with a two vertex truncated dicubane topology endogenously supported by carboxylate-based (2-pyridyl) methylamine ligands: Magneto-structural and DFT studies. *Dalton Trans.* **2023**, *52*, 11922–11933. [CrossRef] [PubMed]
80. Sen, R.; Mondal, K.; dos Santos, M.; Escobar, L.B.L.; Brandão, P.; Reis, M.S.; Lin, Z. A chiral alkali metal capped Ni 4 cubane complex: Synthesis, structure, magnetic and catalytic bromination studies. *J. Mol. Struct.* **2023**, *1274*, 13441. [CrossRef]
81. Scheurer, A.; Ako, A.M.; Saalfrank, R.W.; Heinemann, F.; Hampel, F.; Petukhov, K.; Gieb, K.; Stocker, M.; Müller, P. Synthesis, Magnetic Properties, and STM Spectroscopy of Cobalt (II) Cubanes $[Co^{II}{}_4(Cl)_4(HL)_4]$. *Chem. Eur. J.* **2010**, *16*, 4784–4792. [CrossRef]